https://doi.org/10.1016/j.proci.2014.05.117

A theoretical kinetics study of the reactions of methylbutanoate with hydrogen and hydroxyl radicals

Lidong Zhang, Qinxue Chen and Peng Zhang*

Department of Mechanical Engineering, The Hong Kong Polytechnic University, Kowloon, Hong Kong

Abstract: The chemical kinetics for the reactions of methylbutanoate (MB) with hydrogen and hydroxyl radicals were studied theoretically with the *ab initio* transition state theory. In addition to the hydrogen abstraction reactions of MB by the radicals, the potential energy surfaces of MB+H and MB+OH were further investigated to search for additional significant hydrogen addition channels, which are followed by β-scission reactions to produce non-hydrogen and non-water products, respectively. Stationary points on the potential energy surfaces were calculated at the QCISD(T)/CBS//B3LYP/6-311++G(d,p) level. Phenomenological rate coefficients for temperature- and pressure-dependent reactions were calculated over broad ranges of temperature (200-2500 K) and pressure (1.3×10^{-3}-10^{2} atm) by solving the time-dependent multiple-well master equation. The theoretical rate coefficients were compared with the available experimental and theoretical data and observed discrepancies were analyzed. The predicted rate coefficients are represented in the forms that may readily be used in combustion modeling of MB.

Keywords: Chemical kinetics, Methylbutanoate, Hydrogen radical, Hydroxyl radical, Transition state theory

* Corresponding author.
E-mail: pengzhang.zhang@polyu.edu.hk
Fax: (852)23654703 , Tel: (852)27666664.

1. Introduction

The increasing concerns over energy sustainability, energy security, and climate change have urged an international effort to develop and utilize non-petroleum-based fuels such as biofuels. Biodiesel is one of most widely used biofuels due to its numerous desirable fuel properties. Particularly, biodiesel can replace or blend with petroleum-based diesel for direct use in compression ignition engines and holds potential for improving the engine emission. Because biodiesel is a mixture of long-carbon-chain fatty acid alkyl esters with diverse molecular structures and hence distinct physiochemical properties, the common practice is to simplify the study of biodiesel combustion chemistry to that of single molecule surrogates with shorter carbon chains.

Methylbutanoate (MB, $C_5H_{10}O_2$) has been widely used as a biodiesel surrogate since it has the essential chemical structure, R-C(=O)O-CH_3, while containing a relatively short alkyl chain, $CH_3(CH_2)_2$-. Although it has been recognized that MB is not an ideal surrogate because it does not reproduce well the essential low-temperature chemistry that actual biodiesel exhibits, it can serve as a good starting point for studying larger methyl esters[1]. Furthermore, the chemical kinetics study of biodiesel combustion has been benefitting from the understanding and useful kinetic data gained from the study of MB kinetics[1,2].

Considerable research efforts have been devoted to developing quantitatively accurate reaction mechanism for MB combustion. The first detailed reaction mechanism for MB combustion was established by Fisher et al.[2] and then extensively validated and modified using the experimental data from jet stirred reactors, opposed-flow diffusion flames, flow reactors, shock tubes and rapid compression machines[3-7]. Although these mechanisms show good agreement with experimental data, a number of discrepancies were reported and the accuracy of the reaction mechanisms was found to be sensitive to several typical types of

chain reactions[3-7]. In particular, the reactions between MB and small radicals such as hydrogen and hydroxyl radicals were found to be crucial to predict various combustion parameters at diverse pressure and temperature conditions[1,8].

Whereas the importance of the reactions between MB and hydrogen radical, no direct experimental measurement has been conducted for determining their rate coefficients. Only a few theoretical studies were reported and mostly performed at relatively low levels of computational accuracy. The hydrogen abstraction reactions of MB + H were studied with the BH&HLYP/cc-pvTZ method by Huynh and Violi[9]. The calculated barrier heights for hydrogen abstraction at different sites of MB vary from 6.0 kcal/mol to 8.3 kcal/mol. The CBS-QB3 calculations by Akih-Kumgeh and Bergthorson[10] show that the barrier heights are in the range of 6.5-10.2 kcal/mol. Recently, Liu et al. utilized the high-level CCSD(T)/CBS//B3LYP/6-311++G(d,p) and CCSD(T)/CBS//MP2/cc-pVTZ theoretical methods to study the reactions[8]. Their theoretical barrier heights are in the range of 7.0-10.3 kcal/mol, which is in agreement with the CBS-QB3 results. The theoretical rate coefficients calculated by Liu et al. show substantial discrepancies with not only the previous theoretical predictions but also the previous modeling estimations, especially for the temperature lower than 1000K[2,11,12]. It should be recognized that the theoretical methods employed by Liu et al. are able to predict the rate coefficient with uncertainties about a factor of two and accordingly are more reliable than other theoretical methods of relatively lower computational accuracy. It is interesting and worthwhile to explore the potential energy surface (PES) of MB+H for additional, kinetically significant reaction channels such as the hydrogen addition reactions followed by β-scission reactions, which were assumed to be negligible in the study of Liu et al.

Compared to MB+H, there are even few studies on the reactions between of MB and hydroxyl radical. Most existing reaction mechanisms for MB combustion specify the rate

coefficients for MB+OH by using those derived from the analogous reactions of alkanes. Wallington et al. measured the total reaction rate of MB+OH at the temperature of 296K and the pressure of 25-50 torr by using the flash photolysis resonance fluorescence technique[13]. Le Calvé et al. used the pulsed laser photolysis-laser induced fluorescence technique to measure the total rate of MB+OH over the temperature range of 263-372K and at the pressure of 1.07 bar[14]. By using relative kinetic measurement, Schütze et al. [15] determined the total reaction rate coefficient of MB+OH at 298K, which agrees well with that of Le Calvé et al.. Huynh and Violi theoretically studied the reactions at the level of BH&HLYP/cc-pvtz and the calculated barrier heights for hydrogen abstraction at different sites of MB are in the range of 1.9-6.2 kcal/mol[9]. At the temperature of 298K, the theoretical rate of Huynh and Violi is about two orders of magnitude smaller than the experimental rate coefficients. It is interesting to resolve the substantial discrepancy by using higher level theoretical methods.

Based on the above considerations, we formulated the present theoretical study of the reactions between MB and hydrogen and hydroxyl radicals. The first part of the study is to revisit the reactions between MB and hydrogen radical, with emphasis on exploring the PES of MB+H for additional kinetically favorable reaction channels other than those via hydrogen abstraction and on determining their contribution to the total rate of MB+H. The presence of multiple, interconnected potential wells with multiple dissociation channels necessitates the analysis of a time-dependent, multiple-well Master equation to derive the temperature- and pressure-dependent rate coefficient, especially for the high temperature situation where some of the potential wells equilibrate on the same time scale as that for collisional energy transfer[16-18]. The second part of the study is to determine the reaction rates of MB+OH reactions over a broad range of temperature of 200-2500K with a high-level theory. These calculated rate coefficients are fit to simple functional forms that can be readily incorporated

into the prevalent kinetic modeling codes. The fitted results are expected to be of considerable utility in continuing efforts to validate the oxidation mechanisms of MB.

The theoretical methods used in this study are summarized in Section 2. The results are then presented and discussed in Section 3 and some concluding remarks are made in Section 4.

2. Theoretical Methods

The PESs of the MB+H in the study were first sketched at the level of CBS-QB3[19] and the higher level calculations for the kinetically important reactions were subsequently performed as follows. The geometric structures and vibrational frequencies for stationary points on the PESs were obtained via density functional theory (DFT) employing the Becke three-parameter functional and the Lee-Yang-Parr correlation functional (B3LYP) with the 6-311++G(d,p) basis set[20,21]. The connections of each saddle point to its local minima were examined by using the intrinsic reaction path calculations. Zero-point energy (ZPE) corrections were obtained from the B3LYP/6-311++G(d,p) vibrational frequencies.

Higher level stationary point energies were obtained from QCISD(T) (quadratic configuration interaction with singles doubles and perturbative inclusion of triples) calculations. In previous studies for a similar albeit smaller molecular system[22,23], the QCISD(T) energies calculated with the correlation-consistent, polarized-valence, triple-ζ (cc-pVTZ, denoted by TZ) and quadruple-ζ (cc-pVQZ, denoted QZ) basis sets of Dunning[24,25] were extrapolated to the complete basis set (CBS) limit[26]. This $[QCISD(T)/CBS]_{TZ\rightarrow QZ}$ approach was deemed to be too computationally intensive for the present study. Instead, we used the following alternative method,

$$\mathrm{E[QCISD(T)/CBS]} =$$

$$\mathrm{E[QCISD(T)/CBS]_{DZ\rightarrow TZ}} + \{\mathrm{E[MP2/CBS]_{TZ\rightarrow QZ}} - \mathrm{E[MP2/CBS]_{DZ\rightarrow TZ}}\} \quad (1)$$

which avoids the most time-consuming QCISD(T)/QZ calculation and so are considerably more computationally efficient. The method has been recently examined by Zhang et al. for C_4H_9O system and proved to be an efficient and accurate method for high-level energy estimation[23]. In the present study, all the calculations were performed with the Gaussian 09 program package[27].

For reaction channels with a well-defined transition state, high-pressure rate coefficients were obtained from transition state theory (TST) employing the rigid-rotor harmonic-oscillator (RRHO) approximation for all degrees of freedom except the torsional degrees of freedom. Hindered rotor corrections for the low-frequency torsional modes were obtained from one-dimensional fits to the torsional potentials employing Pitzer-Gwinn-like approximations and the $I^{(2,3)}$ moments of inertia[28]. The fits to the torsional potentials were designed to reproduce the B3LYP/6-311++G(d,p) torsional frequency at the global minimum and the QCISD(T)/CBS// B3LYP/6-311++G(d,p) at local extrema. These fits are considered to provide a simple but reasonably accurate approximation to the internal rotational potentials. One-dimensional tunneling corrections based on asymmetric Eckart potentials were routinely included in all the rate calculations.

For the hydrogen abstraction reactions of MB+OH, a barrierless entrance channel (referred to as the outer transition state) was found to form a vdW complex, as will be shown in Section 3. A saddle point (referred to as the inner transition state) connects the vdW complex to the products. Since the energy of the saddle point is comparable with or even smaller than the energy of MB + OH, the influence of the outer transition state on the rate constants must be considered in the rate calculation. A two-transition-state model, which has

been described in literature [29,30], was consequently used in the present study. An effective transition state number of states for given energy (E) and angular momentum (J), $N_{eff}(E,J)$, is calculated in terms of the transition state number of states at the inner, $N_{inner}(E,J)$, and outer, $N_{outer}(E,J)$, transition states according to the formula:

$$1/N_{eff}(E,J) = 1/N_{inner}(E,J) + 1/N_{outer}(E,J) \quad (2)$$

For the inner TS, the RRHO approximation is reasonably appropriate. For the outer TS, the theoretically simple, while quantitatively accurate long-range TST was adopted, following Georgievskii and Klippenstein[31]. The long-range interaction potential used in the calculation was approximated by a simplified isotropic interaction, $V(R) = -C_6/R^6$, where C_6 can be estimated by $C_6 = 1.5\alpha_1\alpha_2E_1E_2/(E_1+E_2)$, where α_i and E_i (i=1,2) are the polarizability and ionization energy of each fragment, respectively. The estimated C_6 is about 5.4×10^5 $cm^{-1}Å^6$ for MB+OH.

As will be shown in Section 3, the PES of MB+H involves multiple, interconnected potential wells and multiple product channels. The pressure-dependent rate coefficients were determined by solving the time-dependent multi-well master equation, which has been sufficiently described in literature[16-18] and will not be repeated here. The energy transfer probability was approximated by a single-exponential-down model employing the temperature-dependent form $\Delta E_{down} = 200(T/300)^{0.85}$ cm^{-1} for the average downward energy transfer. This approximation has been validated in a related study of C_3H_7O[22]and C_4H_9O[23]. The Lennard-Jones parameters for MB are approximated by σ = 5.85 Å and ε = 227 cm^{-1}. For the bath gas N_2, we used σ = 3.74 Å and ε = 57 cm^{-1}. All the rate calculations were performed by using the VRIFLEX program suite[32].

3. Results and Discussion

3.1 Reactions of MB+H

Many reaction channels were identified on the PES of MB+H (See the Supplement Material, Fig. S1-S5). For simplicity and clarity, only those energetically favorable and then kinetically significant will shown in Fig. 1. The most important reaction channels via direct hydrogen abstraction are listed with increasing barrier heights as follows

$$MB + H \xrightarrow{TS1\text{-}H} MB2J + H_2 \quad R1$$

$$MB + H \xrightarrow{TS2\text{-}H} MB3J + H_2 \quad R2$$

$$MB + H \xrightarrow{TS3\text{-}H} MB4J + H_2 \quad R3$$

$$MB + H \xrightarrow{TS4\text{-}H} MBMJ + H_2 \quad R4$$

which correspond to the hydrogen abstraction from the α, β, γ site of the carbon chain and from the methyl group, respectively. The calculated barrier heights for the reactions were compared with the previous calculation results, as shown in Table 1. It is seen that the present results agree remarkably well with the CCSD(T)/cc-pV∞Z results of Liu et al.[8] and the relative errors are less than 2%. The CBS-QB3 calculation of Akih-Kumgeh and Bergthorson moderately underestimates the energies by about 10%[10]. The BH&HLYP/cc-pvTZ TS energies of Huynh and Violi are about 20% lower than these higher-level energies[9].

Two important hydrogen addition reactions followed by β-scission reactions to non-hydrogen products were identified and shown in Fig. 2:

$$MB + H \xrightarrow{TS5\text{-}H} INT1\text{-}H \xrightarrow{TS6\text{-}H} CH_3OCHO + CH_3CH_2CH_2 \quad R5$$

$$MB + H \xrightarrow{TS7\text{-}H} INT2\text{-}H \xrightarrow{TS8\text{-}H} CH_3CH_2CH_2COOH + CH_3 \quad R6$$

The formation of MB radicals are the rate controlling process which has a energy barrier of 11.10 kcal/mol and 13.90 kcal/mol for R5 and R6, respectively. Since the barrier heights of R5 and R6 are comparable to those of R3 and R4, they hold potential of being an important channels at high temperatures for forming non-hydrogen products. There are another two reaction channels in Fig. 2:

$$INT1\text{-}H \xrightarrow{TS9\text{-}H} INT3\text{-}H \xrightarrow{TS11\text{-}H} INT4\text{-}H \xrightarrow{TS12\text{-}H} CH_3CH_2CH_2CHOH + CH_2O \quad R7$$

$$INT2\text{-}H \xrightarrow{TS10\text{-}H} INT3\text{-}H \xrightarrow{TS11\text{-}H} INT4\text{-}H \xrightarrow{TS12\text{-}H} CH_3CH_2CH_2CHOH + CH_2O \quad R8$$

Since the energy barriers for the isomerization processes are comparable to those of R5 and R6, they may be important channels at high temperatures leading to the formation of formaldehyde and therefore were included in the present rate calculation.

The individual rate coefficients for R1-R4 were fitted as function of temperature and the fitting parameter are presented in Table S1 of Supplementary Material. Only the total rate coefficient of R1-R4 is shown in Fig. 3, mainly for the comparison with the high-level theoretical rate coefficient of Liu et al.[8]. It is seen that the present results are in excellent agreement with those of Liu et al. The small discrepancies occurring below 400K are mainly due to the slightly higher energy barriers in the present theory. The overestimated rate coefficient of Huynh and Violi[9] at intermediate and low temperatures might be due to the obviously lower barrier heights from their calculations. The substantially overshooting rate coefficients of Akih-Kumgeh and Bergthorson [10] may attribute to the overestimated pre-exponential factors in their theory.

An interesting observation of the present multi-well master equation analysis of the PES shown in Fig. 2 is the "well merging" phenomenon, which occurs when the reaction rate from one complex (well) to another chemical species becomes comparable to the rates of its internal energy relaxation due to molecular collisions. Detailed theoretical interpretation and mathematical formulation were given in previous studies[18,23]. In the present study, the dissociation of INT1-H has the smallest energy barrier of 5.67 kcal/mol to the products and is therefore most readily subject to the "well merging" phenomenon as temperature increases. To illustrate the "well merging" phenomenon, the eigenvalues for the chemically significant eigenmodes (CSE)[16-18] and a few of the lowest internal energy relaxation eigenmodes (IERE)[16-18] as functions of temperature at 1 atm pressure are shown in Fig. 4. The solid red line, corresponding to the fastest CSE (denoted by CSE5), represents the dissociation of INT1-H to $CH_3OCHO+CH_3CH_2CH_2$. A bunch of dashed black lines represent the slowest IEREs, which are located at the bottom of the IERE continuum region. As temperature increases to about 400 K, CSE5 merges with the IERE continuum, implying the "merging" of INT1-H to its dissociation products. As a result, the rate coefficient of R5 is completely determined by the transition state TS5-H, and consequently shows pressure-independence for the temperature above 400K, as shown in Fig. 5. As the temperature increases to be about 1000 K, CSE4 merges with the IERE continuum, corresponding to the equilibration of INT2-H with its dissociation products, $CH_3+CH_3CH_2CH_2COOH$. As a result, the rate coefficient of R6 is controlled by TS8-H, and consequently shows pressure-independence for the temperature above 1000K, as shown in Fig. 6. Since increasing the bath gas pressure facilitates the collisional internal energy relaxation while decreasing the pressure suppresses it, it is expected that "well merging" is occurs at higher and lower temperatures if we increase and decrease the bath gas pressure, respectively. As shown in Supplement Material (Fig. S9-S10), the "INT1-H merging" temperature increases to about 500 K and 600K at 10 atm and

100 atm pressure, respectively. The "INT2-H merging" temperature increases to about 1200K and 1500K at 10 atm and 100 atm pressure, respectively. As a result, the rate coefficient curves pronouncedly deviate from that of the rate controlling process at high pressures can be observed in Figs. 5 and 6.

The total rate coefficient of MB+H is dominantly determined by the direct hydrogen abstraction reactions, R1-R4. Although the branching ratio of the four reactions is not less than 0.96 for all the temperature and pressure of interest, the two reactions leading to non-hydrogen products, R5 and R6, account for 3-4% of the total reaction rate when temperature is over 1000K, as shown in Fig. 7. The two reactions leading to the formaldehyde formation, R7 and R8, do not show any significant contribution to the total rate coefficient of MB+H in the entire ranges of pressure and temperatures and consequently can be neglected. It is also noted that R1 is the most important MB+H reaction channel at low temperatures because of its lowest barrier height, all R1-R4 are of roughly the same significance to the total reaction rate at high temperature. Furthermore, R5 is much more important than R6 at low temperatures because of its lower barrier height, while R6 has a higher branching ratio than R5 at high temperatures, mainly due to its looser transition state structure.

3.2 Reactions of MB + OH

The most energetically favorable reactions on the PES of MB+OH are the hydrogen abstraction reactions leading to the H_2O formation, as shown in Fig. 8,

$$MB + OH \rightarrow MB\ldots OH \xrightarrow{TS1\text{-}OH} MB2J + H_2O \quad \text{R9}$$

$$MB + OH \rightarrow MB\ldots OH \xrightarrow{TS2\text{-}OH} MB3J + H_2O \quad \text{R10}$$

$$MB + OH \rightarrow MB\ldots OH \xrightarrow{TS3\text{-}OH} MB4J + H_2O \quad \text{R11}$$

$$MB + OH \rightarrow MB\ldots OH \xrightarrow{TS4\text{-}OH} MBMJ + H_2O \qquad R12$$

which correspond to the hydrogen abstraction from the α, β, γ site of the carbon chain and from the methyl group, respectively. An interesting observation is that TS1-OH has a higher barrier height than that of TS2-OH, which contradicts with the rule of thumb that the α-hydrogen can be more readily abstracted than the β-hydrogen. The underlying physics is the hydrogen bond, which involves the abstracted hydrogen, the hydroxyl radical and the carbonyl oxygen, is stronger in TS2-OH than that in TS1-OH, implying the former is more energetically stabilized. By the same token, we can explain the observed barrier heights for other transition state energies. The molecular structures of the transition states of R9-R12 with the bond lengths and orders of the involving hydrogen bonds are shown in Fig. S12 in the Supplement Material.

Two additional channels leading to non-water products were also identified on the PES of MB + OH:

$$MB + OH \rightarrow MB\ldots OH \xrightarrow{TS5-OH} INT1\text{-}OH \xrightarrow{TS6-OH} CH_3CH_2CH_2{+}CH_3OCOOH \qquad R13$$

$$MB + OH \rightarrow MB\ldots OH \xrightarrow{TS5\text{-}OH} INT1\text{-}OH \xrightarrow{TS7\text{-}OH} CH_3CH_2CH_2COOH{+}CH_3O \qquad R14$$

The rate controlling process of R13 and R14 is the isomerization reaction of the vdW complex to the intemediate species INT1-OH. Although the barrier height of the process is comparable to those of MB+H leading to the non-hydrogen products, it is much larger than those of R9-R12 and hence cannot be kinetically favorable. Consequently, only R9-R12 were included in the present rate calculation.

It is seen that each of the reaction channels R9-R12 consists of a barrierless reaction channel connecting the reactants with the vdW complex, MB...OH, and a lower lying saddle

point connecting the complex with the products. In particular, the energy of the transition state of R10 is even lower than that of MB+OH, implying that the rate controlling process for R10 is the formation of the vdW complex at low temperatures and the saddle point at high temperatures. A two-transition-state theory needs to be used to properly account for the influence of the vdW complex on the rate coefficient, as discussed in the section of "Introduction".

The comparison of the rate coefficients of R9-R12 with the previous theoretical and experimental data is shown in Fig. 9. It is seen that R2 is the dominant channel over a broad range of temperature from 200K to about 1000K. The present theoretical rate coefficients for R2 agree very well with Le Calve et al.'s experimental measurements at 263-372K. It should be noted that the transition state energy of R2 is lowered by 1.0 kcal/mol to lower the theoretical data by a factor of 5 to reproduce the experimental data at 298K. Such an energy adjustment is required to compensate the uncertainties of the calculated barrier height of TS2-OH and the approximate long-range interaction potential and is not uncommon in many previous studies on the similar reaction systems[22,33]. It is also seen that the theoretical results of Huynh and Violi substantially underestimate the rate coefficients by two orders of magnitude at low temperatures. Their results are close to but moderately overshoot the present theoretical results at high temperatures.

The calculated rate coefficient for the reactions discussed above were fitted in the forms that are readily used in combustion modeling of MB. The fitting parameters are listed in Table S1 of Supplementary Material.

4. Concluding Remarks

The chemical kinetics of hydrogen abstraction reactions of methylbutanoate by hydrogen and hydroxyl radicals were studied theoretically with an *ab initio* transition-state-

theory. The master equation analysis was used to investigate the pressure dependence of the additional reaction channels leading to the formation of non-hydrogen products. The theoretical results are in excellent agreement with the limited available experimental data and high-level theoretical data.

For the kinetics of MB+H, two "well merging" phenomena were observed in the master equation analysis and were found to correspond to the equilibration of the INT1-H and INT2-H with their dissociation products, respectively. The "well merging" phenomena were analyzed for their influence on the branching ratio and the pressure-dependent rate coefficients. The dominant reaction channel for MB+H at low temperature is the α-hydrogen abstraction to form MB2J+H_2 because of its lowest energy barrier. With increasing temperature, hydrogen abstraction reactions from other sites become increasingly significant. The hydrogen addition reactions followed by β-scission to non-hydrogen products contribute about 4% of the total rate coefficient of MB+H at high temperatures.

For the kinetics of MB+OH, The most important reaction is the β-hydrogen abstraction leading to MB3J and H_2O. As temperature increases, the contribution from other hydrogen abstraction reactions become increasingly significant. Over a broad temperature range from 300K-2500K, the rate coefficients of the four hydrogen abstraction channels satisfy the following relation: MB3J > MB2J > MBMJ > MB4J.

Acknowledgement

This work was supported by the Hong Kong Research Grants Council/Early Career Scheme (operating under contract number PolyU 5380/13E) and the Shenzhen Science and Technology Innovation Council (SZSTI) (operating under contract number

JCYJ20130401152508650). Lidong Zhang was partly supported by National Key Scientific Instruments and Equipment Development Program of China (2012YQ22011305) and Natural Science Foundation of China (21373193).

Reference

[1] J.Y.W. Lai, K.C. Lin, A. Violi, Prog. Energ. Combust. 37 (2011) 1-14.
[2] E. Fisher, W. Pitz, H. Curran, C. Westbrook, Proc. Combust. Inst. 28 (2000) 1579-1586.
[3] S. Gail, M.J. Thomson, S.M. Sarathy, S.A. Syed, P. Dagaut, P. Dievart, A.J. Marchese, F.L. Dryer, Proc. Combust. Inst. 31 (2007) 305-311.
[4] W. Metcalfe, S. Dooley, H. Curran, J. Simmie, A. EI-Nahas, M. Navarro, J. Phys. Chem. A 111 (2007) 4001-4014.
[5] S. Dooley, H. Curran, J. Simmie, Combust. Flame 153 (2008) 2-32.
[6] S. Walton, M. Wooldrdge, C. Westbrook, Proc. Combust. Inst. 32 (2009) 255-262.
[7] M. Hakka, H. Bennadji, J. Biet, M. Yahyaoui, B. Sirjean, V. Warth, L. Coniglio, O. Herbinet, P. Galaude, F. Billaud, F. Battin-LeClerc, Int. J. Chem. Kinet. 42 (2010) 226-252.
[8] W. Liu, R. Sivaramakrishnan, M.J. Davis, S. Som, D.E. Longman, T.F. Lu, Proc. Combust. Inst. 34 (2013) 401-409.
[9] L.K. Huynh, A. Violi, J. Org. Chem. 73 (2008) 94-101.
[10] B. Akih-Kumgeh, J.M. Bergthorson, Combust. Flame 158 (2011) 1037-1048.
[11] S. Dooley, M. Uddi, S.H. Won, F.L. Dryer, Y.G. Ju, Combust. Flame 159 (2011) 1371-1384.
[12] P. Dievart, S.H. Won, J. Gong, S. Dooley, Y.G. Ju, Proc. Combust. Inst. 34 (2013) 821-829.
[13] T.J. Wallington, P. Dagaut, R. Liu, M.J. Kurylo, Int. J. Chem. Kinet. 20 (1988).
[14] S. Le Calve, G. Le Bras, A. Mellouki, J. Phys. Chem. A 101 (1997) 9137-9141.
[15] N. Schutze, X.Y. Zhong, S. Kirschbaum, I. Bejan, I. Barnes, T. Benter, Atmosph. Environ. 44 (2010) 5407-514.
[16] A. Fernandez-Ramos, J.A. Miller, S.J. Klippenstein, D.G. Truhlar, Chem. Rev. 106 (2006) 4518-4584.
[17] J.A. Miller, S.J. Klippenstein, J. Phys. Chem. A 110 (2006) 10528-10544.
[18] J.A. Miller, S.J. Klippenstein, Phys. Chem. Chem. Phys. 15 (2013) 4744-4753.
[19] J.A. Montgomery Jr., M.J. Frisch, J.W. Ochterski, G.A. Petersson, J. Chem. Phys. 110 (1999) 2822-2827.
[20] A.D. Becke, J. Chem. Phys. 98 (1993) 5648-5652.
[21] R. Krishnan, J.S. Binkley, R. Seeger, J.A. Pople, J. Chem. Phys. 72 (1980) 650-654.
[22] J. Zador, A.W. Jasper, J.A. Miller, Phys. Chem. Chem. Phys. 11 (2009) 11040-11053.
[23] P. Zhang, S.J. Klippenstein, C.K. Law, J. Phys. Chem. A 117 (2013) 1890-1906.
[24] T.H. Dunning, J. Chem. Phys. 90 (1989) 1007-1023.
[25] R.A. Kendall, T.H. Dunning, R.J. Harrison, J. Chem. Phys. 96 (1992) 6796-6806.
[26] J.M.L. Martin, O. Uzan, Chem. Phys. Lett. 282 (1998) 16-24.
[27] M.J. Frisch, G.W. Trucks, H.B. Schlegel, G.E. Scuseria, M.A. Robb, J.R. Cheeseman, G. Scalmani, V. Barone, B. Mennucci, G.A. Petersson, H. Nakatsuji, M. Caricato, X. Li, H.P. Hratchian, A.F. Izmaylov, J. Bloino, G. Zheng, J.L. Sonnenberg, M. Hada, M. Ehara, K. Toyota, R. Fukuda, J. Hasegawa, M. Ishida, T. Nakajima, Y. Honda, O. Kitao, H. Nakai, T. Vreven, J.A. Montgomery Jr., J.E. Peralta, F. Ogliaro, M. Bearpark, J.J. Heyd, E. Brothers, K.N. Kudin, V.N. Staroverov, R. Kobayashi, J. Normand, K. Raghavachari, A. Rendell, J.C. Burant, S.S. Iyengar, J. Tomasi, M. Cossi, N. Rega, J.M. Millam, M. Klene, J.E. Knox, J.B. Cross, V. Bakken, C. Adamo, J. Jaramillo, R. Gomperts, R.E. Stratmann, O. Yazyev, A.J. Austin, R. Cammi, C. Pomelli, J.W. Ochterski, R.L. Martin, K. Morokuma, V.G. Zakrzewski, G.A. Voth, P. Salvador, J.J. Dannenberg, S. Dapprich, A.D. Daniels, O. Farkas, J.B.

Foresman, J.V. Ortiz, J. Cioslowski, D.J. Fox, Gaussian 09, Gaussian, Inc., Wallingford CT, 2009.
[28] A.L.L. East, L. Radom, J. Chem. Phys. 106 (1997) 6655-6674.
[29] E.E. Greenwald, S.W. North, Y. Georgievskii, S.J. Klippenstein, J. Phys. Chem. A 109 (2005) 6031-6044.
[30] H. Sabbah, L. Biennier, I.R. Sims, Y. Georgievskii, S.J. Klippenstein, I.W.M. Smith, Science 317 (2007) 102-105.
[31] Y. Georgievskii, S.J. Klippenstein, J. Chem. Phys. 122 (2005) 194103.
[32] S.J. Klippenstein, A.F. Wagner, R.C. Dunbar, D.M. Wardlaw, S.H. Robertson, J.A. Miller, Variflex, Argonne National Laboratory (2007).
[33] J. Daranlot , A. Bergeat , F. Caralp , P. Caubet , M. Costes , W. Forst , J.-C. Loison , K.M. Hickson ChemPhysChem 11 (2010) 4002-4010.

Table 1: Calculated barrier heights for R1-R4 of MB+H (kcal/mol).

Reaction	Present work	Reference[8]	Refernce[9]	Reference[10]
R1	7.10	6.97	6.0	6.54
R2	8.29	8.10	6.5	7.62
R3	10.20	10.09	8.3	10.02
R4	10.37	10.32	8.4	9.83

Figure Captions

(Color figures in electronic version only)

Figure 1: PES of the hydrogen abstraction reactions of MB+H at the QCISD(T)/CBS//B3LYP/6-311++G(d,p) level.

Figure 2: PES of the hydrogen addition reactions of MB+H at the QCISD(T)/CBS//B3LYP/6-311++G(d,p) level.

Figure 3: The high-pressure limit of the total reaction rate of the hydrogen abstraction reactions of MB+H.

Figure 4: Chemically significant eigenvalues (CSEs) and internal energy relaxation eigenvalues (IEREs) for H-addition reactions of MB+H as functions of temperature at 1atm.

Figure 5: Pressure-dependent rate coefficients of MB+H→CH_3OCHO+$CH_3CH_2CH_2$.

Figure 6: Pressure-dependent rate coefficients of MB+H→$CH_3CH_2CH_2COOH$+CH_3.

Figure 7: Branching ratios of the reactions on the PES of MB+H.

Figure 8: PES of MB+OH at the QCISD(T)/CBS//B3LYP/6-311++G(d,p) level.

Figure 9: Rate coefficients of the hydrogen abstraction reactions on the PES of MB+OH.

Figure 1

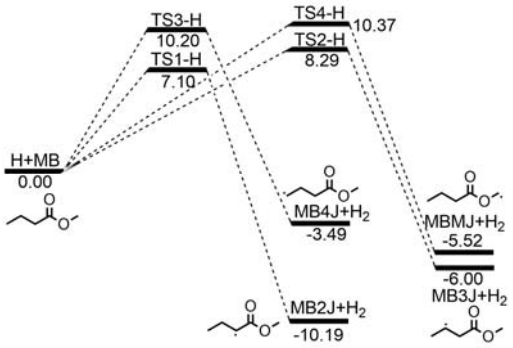
TS3-H
10.20
TS4-H
10.37
TS2-H
8.29
TS1-H
7.10
H+MB
0.00
MB4J+H2
-3.49
MBMJ+H2
-5.52
-6.00
MB3J+H2
MB2J+H2
-10.19

Figure 2

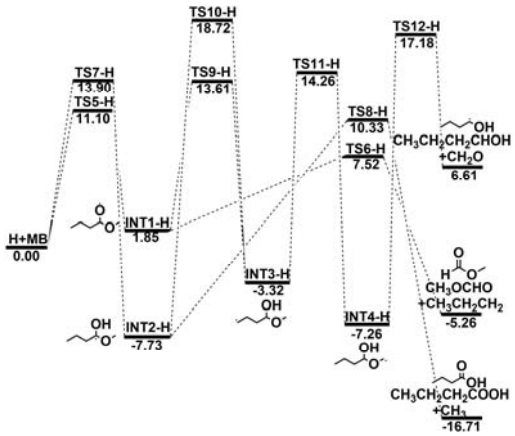
TS10-H
18.72
TS12-H
17.18
TS7-H
13.90
TS9-H
13.61
TS11-H
14.26
TS5-H
11.10
TS8-H
10.33
CH3CH2CH2CHOH
+CH2O
6.61
TS6-H
7.52
H+MB
0.00
INT1-H
1.85
INT3-H
-3.32
CH3OCHO
+CH3CH2CH2
-5.26
INT2-H
-7.73
INT4-H
-7.26
CH3CH2CH2COOH
+CH4
-16.71

Figure 3

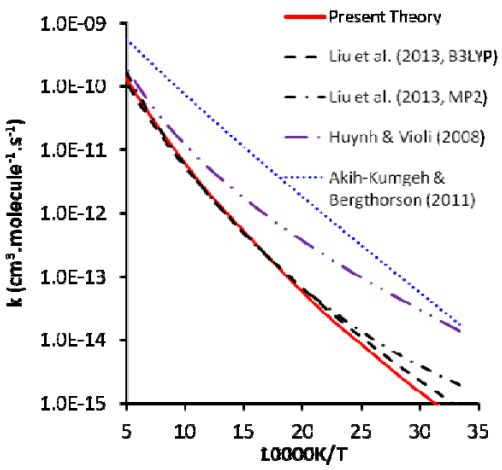
Present Theory
Liu et al. (2013, B3LYP)
Liu et al. (2013, MP2)
Huynh & Violi (2008)
Akih-Kumgeh & Bergthorson (2011)
k (cm³.molecule⁻¹.s⁻¹)
1.0E-09
1.0E-10
1.0E-11
1.0E-12
1.0E-13
1.0E-14
1.0E-15
5
10
15
20
25
30
35
10000K/T

Figure 4

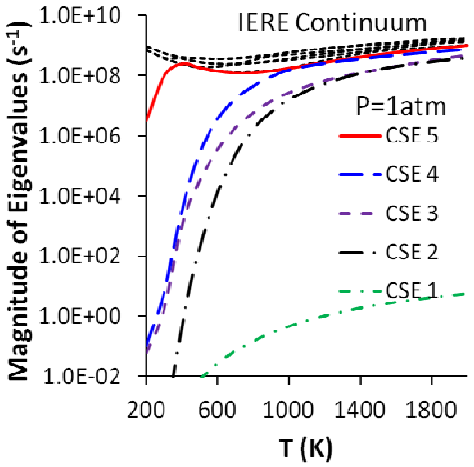
IERE Continuum
P=1atm
CSE 5
CSE 4
CSE 3
CSE 2
CSE 1
Magnitude of Eigenvalues (s-1)
1.0E+10
1.0E+08
1.0E+06
1.0E+04
1.0E+02
1.0E+00
1.0E-02
200
600
1000
1400
1800
T (K)

Figure 5

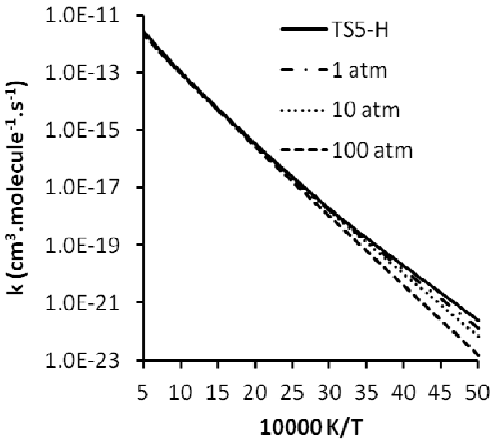
1.0E-11
1.0E-13
1.0E-15
1.0E-17
1.0E-19
1.0E-21
1.0E-23
k (cm³.molecule⁻¹.s⁻¹)
5 10 15 20 25 30 35 40 45 50
10000 K/T
TS5-H
1 atm
10 atm
100 atm

Figure 6

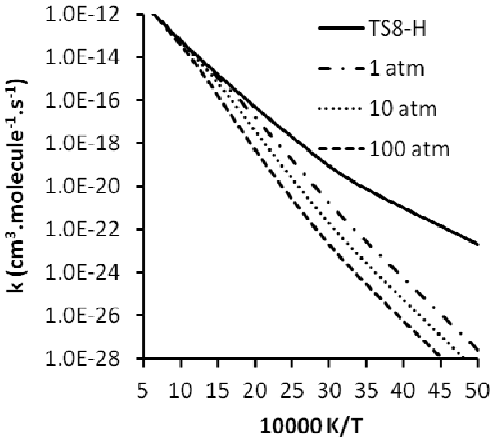
1.0E-12
1.0E-14
1.0E-16
1.0E-18
1.0E-20
1.0E-22
1.0E-24
1.0E-26
1.0E-28
k (cm³.molecule⁻¹.s⁻¹)
5 10 15 20 25 30 35 40 45 50
10000 K/T
TS8-H
1 atm
10 atm
100 atm

Figure 7

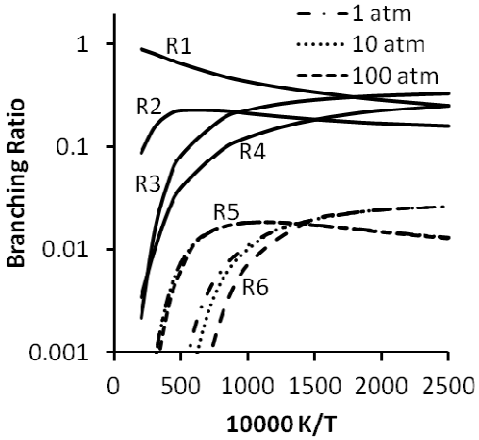
1 atm
10 atm
100 atm
R1
R2
R3
R4
R5
R6
Branching Ratio
1
0.1
0.01
0.001
0
500
1000
1500
2000
2500
10000 K/T

Figure 8

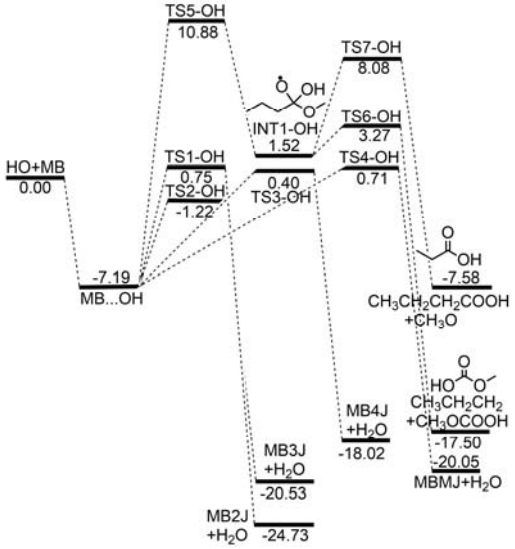
TS5-OH
10.88
TS7-OH
8.08
INT1-OH
1.52
TS6-OH
3.27
HO+MB
0.00
TS1-OH
0.75
TS2-OH
-1.22
0.40
TS3-OH
TS4-OH
0.71
-7.19
MB...OH
-7.58
CH3CH2CH2COOH
+CH3O
HO
CH3CH2CH2
+CH3OCOOH
-17.50
MB4J
+H2O
-18.02
MB3J
+H2O
-20.53
-20.05
MBMJ+H2O
MB2J
+H2O
-24.73

Figure 9

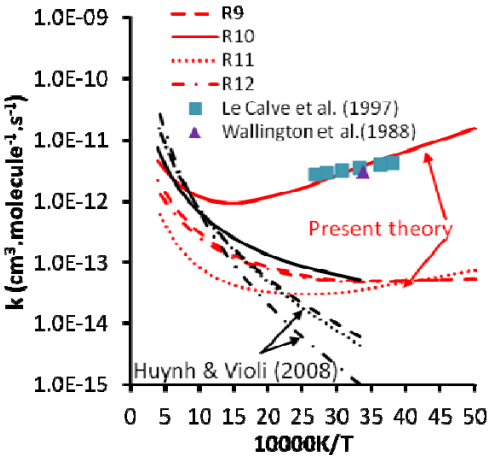
R9
R10
R11
R12
Le Calve et al. (1997)
Wallington et al.(1988)
Present theory
Huynh & Violi (2008)
k (cm³.molecule⁻¹.s⁻¹)
1.0E-09
1.0E-10
1.0E-11
1.0E-12
1.0E-13
1.0E-14
1.0E-15
0 5 10 15 20 25 30 35 40 45 50
10000K/T

Supplemental Materials

Item	Filename	Content
1	Supplementary material.doc	The calculated PESs of MB+H at the CBS-QB3 level. The rate constants and fitting parameters The molecular properties from theoretical calculations.